Energetic Mapping of Ni Catalysts by Detailed Kinetic Modeling†

Erlend Bjørgum, De Chen, Mari Grande Bakken, Kjersti Omdahl Christensen, and Anders Holmen*

Department of Chemical Engineering, Norwegian University of Science and Technology (NTNU), N-7491 Trondheim, Norway

Ole Lytken and Ib Chorkendorff

Interdisciplinary Research Center for Catalysis (ICAT), Department of Physics and Department of Chemical Engineering, Technical University of Denmark, DK-2800 Lyngby, Denmark

Received: March 15, 2004; In Final Form: August 2, 2004

Temperature-programmed desorption (TPD) of CO has been performed on supported and unsupported nickel catalysts. The unsupported Ni catalyst consists of a Ni(14 13 13) single crystal which has been studied under ultrahigh vacuum conditions. The desorption energy for CO at low CO surface coverage was found to be 119 kJ/mol, and the binding energy of C to the Ni(111) surface of the crystal was 703 kJ/mol. The supported catalysts consist of nickel supported on hydrotalcite-like compounds with three different Mg^{2+}/Al^{3+} ratios. The experimental results show that for the supported Ni catalysts TPD of CO leads to desorption of both CO and CO_2, with the latter being dominant. Dissociation of CO takes place, and considerable amounts of residue C are left on the surface. The residue C is removed by temperature-programmed oxidation (TPO). The results show that a low Mg^{2+}/Al^{3+} ratio in the hydrotalcite precursor seems to result in more steplike sites, kinks, and defects for carbon monoxide dissociation. A detailed kinetic modeling of the TPO results based on elementary reaction steps has been conducted to give an energetic map of supported Ni catalysts. Experimental results from the ideal Ni surface fit nicely with literature values, providing useful information for identifying active sites on supported Ni catalysts.

Introduction

Steam reforming of hydrocarbons on Ni catalysts is a main process for production of synthesis gas.[1] Unfortunately, steam reforming suffers from the possible risk of coke formation.[1−3] Different approaches have been proposed for reducing the risk of coke formation such as the use of Ni/Mg−Al catalysts. These catalysts can be obtained by thermal decomposition of synthetic hydrotalcite anionic clays followed by reduction.[4] Synthetic Mg−Al layered double hydroxide materials similar to the naturally occurring hydrotalcite ($[Mg_6Al_2(OH)_{16}]CO_3{\cdot}4H_2O$) have many applications due to their unique physiochemical properties.[5] Of particular interest for the use of hydrotalcites as catalysts are the high surface area and the formation of homogeneous mixtures of oxides with very small crystal size stable to thermal treatments, which by reduction form small and thermally stable metal crystallites giving a highly dispersed metal.[6] The nonacidic nature of these materials is also very important.

Temperature-programmed desorption (TPD) of CO is often used to give detailed information on the mechanism of adsorption and adsorption heat. The adsorption heat of CO is directly related to the binding energy of carbon to Ni, which is an indication of the strength of the metallic active sites. The dissociative nature of CO adsorption on Ni is an important step in reactions involving synthesis gas.[7] Several investigations have concluded that CO dissociation (and carbon formation) takes place at steps or defect sites on the catalysts.[7−10] Moreover, Chen et al.[11] show that the carbon binding energy is the most important parameter for microkinetic modeling of the kinetic behavior of steam methane reforming on Ni catalysts. The distribution of binding energies of carbon to the Ni catalysts will therefore provide valuable information about its use for methane steam reforming.

The present work deals with CO adsorption on well-defined systems (single crystals) and on supported catalysts. TPD of CO adsorbed on a Ni single crystal with about 4% steps was performed to investigate the effect of steps upon the adsorption of CO on Ni(111). TPD and temperature-programmed oxidation (TPO) were used to study the kinetics and mechanism of CO adsorption/desorption on different supported Ni catalysts. TPO was used to find the amount of residue carbon on the surface after CO desorption, and the TPO experiments are modeled using a microkinetic approach aiming at mapping the distribution of carbon binding energies on the catalysts.

Microkinetic analysis is an examination of catalytic reactions in terms of elementary chemical reactions steps occurring on the catalytic surface and their relation with each other and with the surface during a catalytic cycle.[12] Previously, the rate constants were extracted from rate equations obtained by fitting kinetic data. In a microkinetic analysis, they are calculated by computational chemistry or measured by surface science techniques where only a few sensitive parameters are normally optimized to fit experimental values.[13] One way to estimate the activation energies of the elementary steps on the catalytic surface is by using the BOC-MP (bond order conservation-

† Part of the special issue "Michel Boudart Festschrift".

* To whom correspondence should be addressed. E-mail: Anders.Holmen@chemeng.ntnu.no.

10.1021/jp048850e CCC: $30.25 © 2005 American Chemical Society
Published on Web 10/09/2004

TABLE 1: Catalyst Composition and General Information from the XRD Experiments

catalyst	NiO[a] [%]	MgO[a] [%]	Al_2O_3[a] [%]	x[b]	c, interlayer distance[c] [Å]
HT30		29.1	60.9	0.68	22.85
HT50		50.7	49.3	0.46	22.80
HT70		70.7	29.3	0.27	23.27
NiOHT30	15.9	24.5	59.6		26.60
NiOHT70	15.9	59.5	24.6		25.10

[a] Data from Condea. [b] x is the ratio between Al^{3+} and Mg^{2+} in the hydrotalcite structure. [c] Calculated from XRD spectra.

Morse potential) approach.[14] By using BOC theory, different activation energies can be calculated for different binding energies of the elements involved. This theory creates a link between the bond strength and activation energies, which can provide direct guidance for suggesting new catalysts or improving existing ones.[2]

Experimental Section

Catalyst Preparation. The supported nickel catalysts containing 12.5 wt % Ni were prepared by incipient wetness impregnation on different supports with aqueous solutions of $Ni(NO_3)_2 \cdot 6H_2O$. Three different hydrotalcite supports from Condea were used in this study: HT30, HT50, and HT70. The numbers 30, 50, and 70 indicate the wt % of MgO compared to Al_2O_3 in the hydrotalcite. Catalyst composition and structural data are given in Table 1. The hydrotalcites were dried for 24 h at 373 K both before and after impregnation and then calcined in air at 873 K for 4 h.

X-ray Diffraction (XRD). X-ray diffraction studies were performed in a Siemens D5005 powder X-ray diffractometer using monochromatic Cu Kα radiation with a wavelength of 1.54 Å. The measurements were done on calcined catalysts, and average NiO particle sizes were calculated from the most intense NiO line, using the Scherrer formula.[15]

Temperature-Programmed Reduction (TPR). The TPR instrumentation has been described elsewhere.[16] The U-shaped tubular quartz reactor was loaded with 0.2−0.4 g of catalyst and heated at a rate of 4 K/min to 1173 K with a gas consisting of 7% H_2 in Ar. The gas flow rate was 50 mL/min.

Volumetric H_2 Chemisorption. H_2 adsorption isotherms were measured at 308 K using a Micromeritics ASAP 2010 capable of a vacuum of 10^{-5} Torr or better. The reactor was loaded with 1 g of catalyst. Prior to the chemisorption measurements, the catalyst samples were reduced in situ in flowing hydrogen at 903 K for 12 h. After reduction, the samples were evacuated for 0.5 h at 903 K before cooling to 308 K.

The adsorption isotherms were measured between 10 and 510 Torr. After pumping for 30 min, a second isotherm was measured in order to separate strongly and weakly held hydrogen. Only the strongly adsorbed hydrogen is reported here. By extrapolation of the linear part of the isotherms to zero pressure, the amount of hydrogen chemisorbed is determined.

TPD Experiments under Ultrahigh Vacuum Conditions. The apparatus used is a standard ultrahigh vacuum (UHV) chamber with a base pressure below 10^{-10} Torr, equipped with a 3 kV electron gun and a cylindrical mirror analyzer for Auger electron spectroscopy (AES), a quadrupole mass spectrometer designed for TPD, an ion gun used for Ar^+ sputtering, and several leak valves for dosing gas. The sample is spot-welded between two 0.5 mm tungsten wires and can be resistively heated through the same. The temperature can be monitored by a chromel−alumel thermocouple spot-welded to the side of the sample. A liquid nitrogen reservoir allowed for cooling to 83 K. A more thorough description of the apparatus can be found elsewhere.[17]

The sample used was a 10 mm Ni(111) single crystal supplied by Metal Crystals & Oxides Ltd. misaligned by 2° with a accuracy of 0.5° toward the (100) creating a Ni(14 13 13) surface with approximately 4% (100) type steps. The sample was cleaned by 1 kV Ar^+ ion sputtering at 500 K, annealed at 1273 K for 2 min, oxidized in 2.0×10^{-7} Torr O_2 at 550 K for 5 min, and reduced in 5.0×10^{-7} Torr H_2 at 623 K for 15 min. The cleaning procedure was checked with AES, and no impurities could be detected.

TPD/TPO Experiments under Flow Conditions. The TPD and TPO studies were done using a U-shaped tubular quartz reactor with the catalyst sample fixed on a sinter. An electrical furnace was used to heat the quartz reactor, and the product composition was followed by on-line mass spectrometry (MS).

The reactor was loaded with approximately 0.9 g of catalyst. The flow was kept constant at 25 mL/min during all experiments, using Ar as an inert gas, and all experiments were performed under atmospheric pressure. The catalyst was reduced in a mixture of 11 mL/min H_2 and Ar heated from ambient to 923 K at a rate of 5 K/min and kept at this temperature for 10 h. After reduction, the samples were flushed for 0.5 h with Ar at 923 K before cooling to 328 K. A mixture of 11 mL/min CO and Ar was dosed at 328 K until a stable mass signal for CO was obtained. The flow was then switched to Ar.

TPD involved heating the sample from 328 to 923 K at a rate of 10 K/min. After the TPD, the sample was cooled to 328 K. At this temperature, the flow was switched to 11 mL/min O_2 and Ar. TPO was performed when the MS signals for CO and CO_2 were stable and involved heating the sample from 328 to 973 K at a rate of 10 K/min.

Microkinetic Modeling and Determination of Kinetic Parameters. For the TPD experiments performed under UHV conditions, the activation energy of CO desorption and the preexponential factor were estimated by using an Arrhenius plot at low surface coverage.

All the modeling is done using MATLAB. Shustorovich[18] has reviewed in detail the method and the equations for calculating heat of chemisorption and activation barriers using the BOC theory. All the activation energies in this work are calculated using the BOC method. The initial preexponential factors were either taken from Chen et al.[2] or estimated by transition-state theory. The preexponential factors for the adsorption steps were calculated using collision theory and sticking coefficients, s_0:

$$k_A = \frac{s_0(T)}{\sqrt{2\pi m_A k_B T}} \tag{1}$$

Dumesic et al.[12] summarized typical ranges for the preexponential factor used in microkinetic analysis.

The TPO experiments in the flow reactor are modeled with the reactions and rate constants given in Table 2. The flow reactor is modeled as a continuously stirred tank reactor (CSTR):[12]

$$\frac{dF_i}{dt} = F_i^0 - F_i + N_i\sigma \tag{2}$$

where F_i is the flow of component i (mol/s), F_i^0 is the initial flow (mol/s), N_i is the turnover frequency (1/catalytic sites, s), and σ a constant (mol, catalytic sites). ($\sigma = w_{cat}Df_{Ni}/M_{Ni}$ where

TABLE 2: Microkinetic Model for TPO Experiments[a]

	reaction	rate constant, forward reaction	rate constant, reverse reaction
r_1	$O_2 + 2^* \leftrightarrow 2O^*$	$3.5 \times 10^7\ e^{-12500/RT}$	$1.0 \times 10^{13}\ e^{-77300/RT}$
r_2	$^{**}C + ^*O \leftrightarrow ^{**}CO + ^*$	$1 \times 10^{13}\ e^{-143000/RT}$	$1 \times 10^{13}\ e^{-144000/RT}$
r_3	$^{**}CO \leftrightarrow CO + 2^*$	$5 \times 10^{12}\ e^{-122300/RT}$	$s_0 = 1$
r_4	$^{**}CO + ^*O \leftrightarrow ^{**}CO_2 + ^*$	$2.2 \times 10^{14}\ e^{-71200/RT}$	$1.2 \times 10^{12}\ e^{-26300/RT}$
r_5	$^{**}CO_2 \leftrightarrow CO_2 + 2^*$	$1 \times 10^{13}\ e^{-27300/RT}$	$s_0 = 0.02$

[a] The adsorption steps are described by the sticking coefficient s_0. Activation energies are given in J/mol, and the gas constant R in J/(K mol). All activation constants in the table are calculated using BOC and a binding energy of C to Ni of 715 kJ/mol. When the binding energy of C−Ni is changed or adjusted, the E_A value will change.

w_{cat} is the catalyst weight (g), D is the dispersion, f_{Ni} is g Ni/g catalyst, and M_{Ni} is the molecular weight of Ni.)

Four surface species (C*, O*, **CO, **CO_2) and three gas-phase components (CO, CO_2, O_2) were modeled by four surface species mass balance equations and three mass balance equations for the reactor, respectively. Equation 2 is used for the mass balance of gas components over the reactor, while eq 3 is used for the surface species mass balance:

$$\frac{d\theta_i}{dt} = \sum \alpha_i r_j \tag{3}$$

where θ_i is the surface coverage of component i, α_i is the stoichiometric factor for component i, and r_j is the reaction rate of elementary step j (elementary steps are listed in Table 2).

The modeling of the TPO experiments was done by modeling single TPO peaks at given binding energies of carbon to nickel. By changing this binding energy, one can calculate new activation energies for the elementary steps using BOC, and new peaks are obtained. Once several peaks are modeled, the peaks can be weighted to fit the experimental data, giving a distribution of carbon binding energies on the catalyst.

The TPO model is fitted to the experimental results. The mass ratio of CO_2/CO desorption was high, and therefore the main result from the model is the CO_2 desorption. During TPD under UHV conditions, no CO_2 was observed as the CO pressure in these experiments was always very low. The lack of CO_2 during the UHV experiments is discussed later.

Results and Discussion

Characterization: XRD. According to Cavani et al.,[6] a hydrotalcite structure is defined by the ratio x, which is the ratio between Al^{3+} and Mg^{2+} in the hydrotalcite structure ($x = Al^{3+}/(Mg^{2+}+Al^{3+})$). Many indications show that it is possible to obtain pure hydrotalcites only for $0.2 \le x \le 0.33$. For x values outside the above range, either the pure hydroxides or other compounds with different structures have been obtained. In some cases, the formation of pure hydrotalcites has also been reported when operating with excess Al. In these cases, it is most likely that also the formation of amorphous $Al(OH)_3$ (not detectable by XRD) occurred due to the increased number of neighboring Al octahedra.[6]

The XRD curve given in Figure 1a for HT70 fits nicely with a hydrotalcite structure with a Mg/Al ratio of about 3. The HT70 catalyst also has an x value of 0.27 (see Table 1). The peaks observed at 2θ angles of around 11, 22, 35, and 61° (indicated by (*) in Figure 1) are the fingerprints of hydrotalcites or hydrotalcite-like compounds.[19]

The HT50 and HT30 catalysts have x values of 0.46 and 0.68, respectively. This XRD data fit better to a hydrotalcite-like compound, with a lower Mg/Al ratio. The peaks are smaller and wider compared to those of the HT70 catalyst, indicating a less crystalline structure and smaller particles. For the HT30 catalyst, peaks are observed at 2θ angles of 15, 28, 39, and 50° (indicated by (○) in Figure 1) which are not present for the two other catalysts. The XRD database indicates that it could be some aluminum oxide structures.

When calculating the distance between the layers in the hydrotalcite (the factor c), we see a trend as also reported by Cavani et al.[6] with a lowering of the distance between the layers with increased x value. The data are given in Table 1. Figure 1b shows the XRD spectra for the Ni-impregnated hydrotalcite precursors after drying at 373 K for 24 h. The displacement of the hydrotalcite peaks in the spectra is easily observed. The first hydrotalcite peak is moved from 11.7 to 10.0° for HT30 and from 11.4 to 10.5° for HT70. The interlayer distance between the hydrotalcite layers is now greater for HT30 (26.6 Å) compared to HT70 (25.1 Å) (see Table 1). This could be an indication of an anion exchange in the hydrotalcite layers. According to Cavani et al.,[6] this trend is observed when the anion between the layers is nitrate, NO_3^-. The reason for the changes in the layer distances is related both to the necessity of a larger amount of monovalent ion for positive charge compensation and to the greater space occupied in the interlayer as compared to CO_3^{2-} ions. Another possible explanation for the changes in interlayer distances could be incorporation of Ni^{2+} ions in the layers. This is discussed further under the TPR results.

For the calcined nickel catalysts shown in Figure 1c, the hydrotalcite structures are lost. NiO, MgO, and a Ni/Mg−O solid metal solution give peaks at 37, 43, 63, 75, and 79°, with the largest peak at 43°. Because the peaks are overlapping, it is difficult to say whether they consist of NiO, MgO, and/or Ni/Mg−O.

For the NiOHT30 catalyst, we observed phases which could be spinel phases, $NiAl_2O_4$ or $MgAl_2O_4$, or some solid oxide metal solution (Ni/Mg−O) at 45 and 66°. It is known[20] that spinel phases could be present when calcination takes place at temperatures above 1023 K. Temperature gradients during the calcination could lead to higher temperatures than the calcination temperature of 873 K. The NiOHT30 catalyst also shows broader peaks with a higher degree of noise. This indicates that the catalyst consists of small amorphous particles. The large peak at 45° could also be Ni metal.

Based on the XRD spectra, the average NiO particle sizes are calculated using the Scherrer formula, and the results are given in Table 3. The results in Table 3 show an increase in the particle size with increasing Mg^{2+}/Al^{3+} ratio in the hydrotalcite precursor.

Characterization: Chemisorption. The H_2-chemisorption data together with the particle sizes calculated from the dispersion data are given in Table 3. The nickel particle sizes calculated by chemisorption show the same trend as the XRD-based calculations (Table 3). These values are also similar for the NiOHT50 and the NiOHT30 catalysts. For the NiOHT70 catalyst, however, chemisorption gives smaller particles sizes compared to the XRD calculations.

Table 3 clearly shows the large difference between NiOHT30 and the two other catalysts. The Ni surface area is about twice as large compared to the two others.

TPR. The TPR results of the different catalysts are shown in Figure 2. The NiOHT50 and NiOHT70 catalysts have one large peak at around 670 K. The NiOHT50 catalyst also has a shoulder on the left side of the peak. All three catalysts have a peak in the area 1050−1100 K.

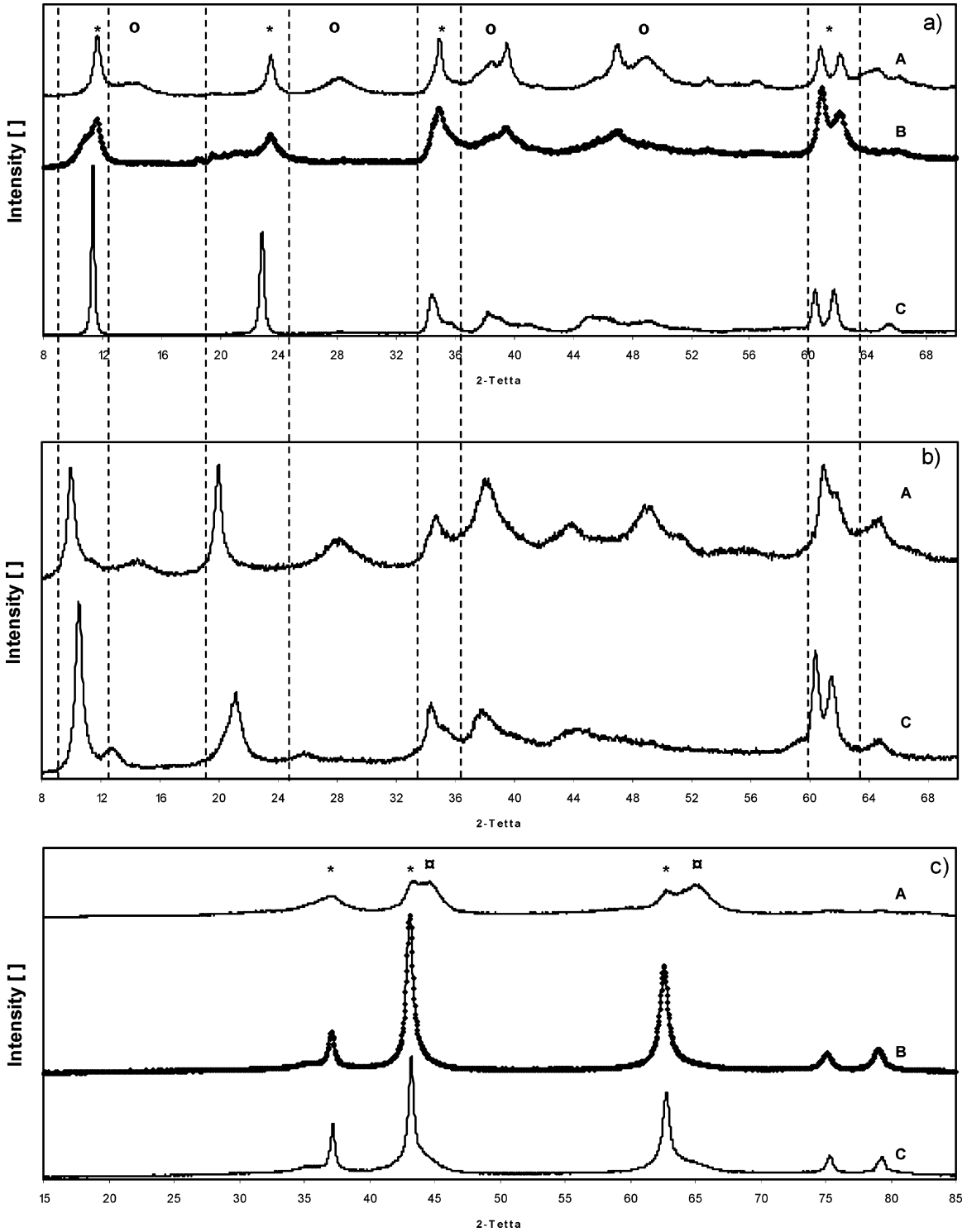

Figure 1. Panels a and b show XRD patterns of the precursor materials where (*) denotes reflections of hydrotalcite-type structures and (○) denotes reflections of some aluminum oxide structures. In panel b, HT30 and HT70 are impregnated with Ni: (A) HT30, (B) HT50, (C) HT70. Panel c shows XRD patterns of NiO supported on calcined hydrotalcite precursors where (*) denotes reflections of Ni/Mg−O structures and (-☼-) denotes possible spinel structures: (A) NiOHT30, (B) NiOHT50, (C) NiOHT70.

TABLE 3: Ni Surface Area, Dispersion Data, and Ni Particle Sizes for the Supported Catalysts

catalyst	Ni metal surface area [m^2 Ni/g_{cat}]	dispersion [%]	particle size from chemisorption [nm]	particle size from XRD [nm]	carbon residue after TPD [mmol/m^2Ni]
NiOHT30	7.2	8.6	12	12	5.4
NiOHT50	3.7	4.5	23	24	5.3
NiOHT70	3.5	4.2	24	29	2.6

The reduction peak at low temperature is believed to be reduction of NiO.[21] The wide peaks at 1050−1100 K are most likely reduction of a Ni^{2+} divalent mixed metal oxide phase, NiO−MgO.[22]

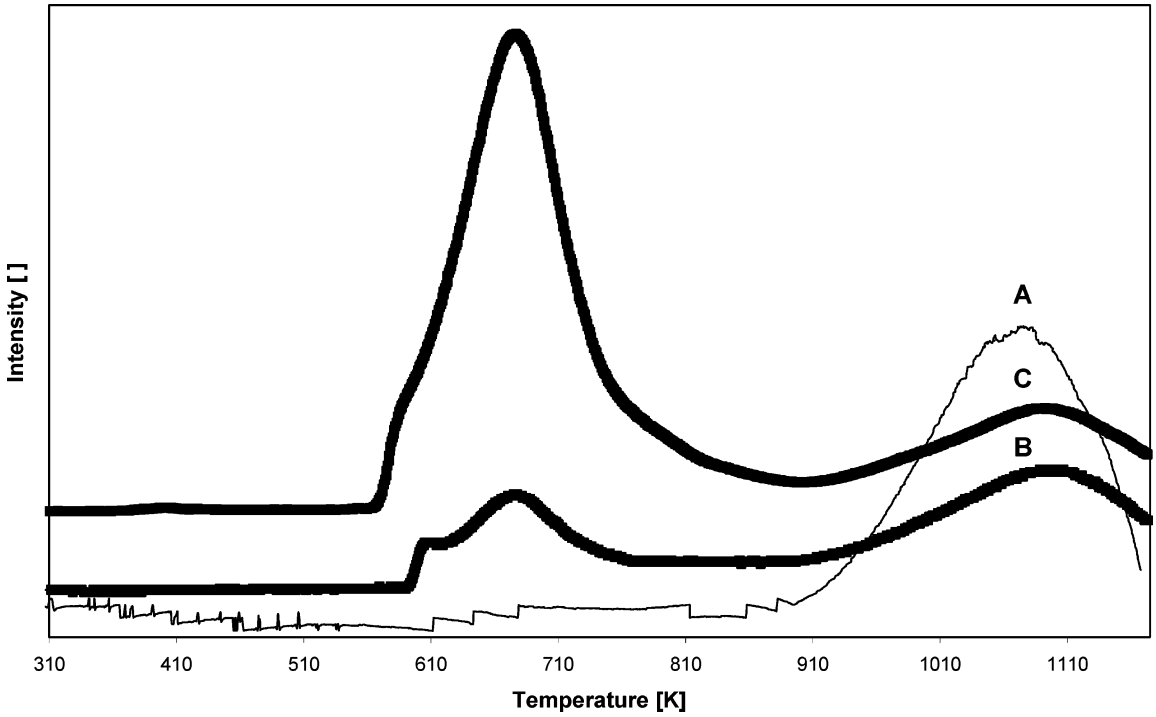

Figure 2. TPR of the NiO/HT catalysts: (A) NiOHT30, (B) NiOHT50, (C) NiOHT70.

As shown in Figure 2, the results indicate a lowering of the fraction of easily reducible NiO when lowering the Mg^{2+}/Al^{3+} ratio. The high temperature peak is of the same size for the NiOHT50 and NiOHT70 catalysts, but for the NiOHT30 catalyst the reduction temperature is slightly lower and the peak is also larger compared to the other two.

Schulze et al.[22] found that calcined hydrotalcites containing Al, Mg, and Ni had only one reduction peak, corresponding to the reduction of Ni^{2+} in a divalent mixed metal oxide phase (NiO−MgO). They found that the lower the Ni/Mg ratio in the hydrotalcites, the more difficult it became to reduce them. Fornasari et al.[20] also observed a decrease in the reducibility of the Ni^{2+} ions with increasing Mg^{2+} content in a calcined Ni/Mg/Al structure, which was attributed to the presence of foreign ions (Mg^{2+} and/or Al^{3+}) inside the NiO phase.

The difference in the fraction of NiO in the TPR spectra for the three catalysts can possibly be explained by the incorporation of Ni into the hydrotalcite structure. For the NiOHT30 catalyst, the lack of a reduction peak for NiO indicates that NiO is not easily reducible and that the Ni here must be found in some kind of mixed oxide phase. During impregnation the Ni may be settled inside the hydrotalcite layers, and after calcination Ni is more incorporated into the structure.[23] Ni exists in mixed metal oxide form together with Mg, and Ni is better dispersed compared to the other two catalysts (see chemisorption data, Table 3).

The reason for the lower temperature for the second reduction peak for the NiOHT30 catalyst, compared to the other two, can according to Schulze et al.[22] be the low Mg^{2+}/Ni^{2+} ratio. This reduction peak being larger for NiOHT30 also indicates that more of the Ni is strongly bonded in a mixed metal oxide form together with Mg.

For the NiOHT50 and NiOHT70 catalysts, more NiO is available on the surface for reduction. The trend is that the higher Mg^{2+}/Al^{3+} ratio of the hydrotalcite precursor leads to lower dispersion of the Ni in the calcined catalyst and higher reducibility.

TPD of CO on Nickel Single Crystal. Temperature-programmed desorption of CO was performed on the Ni model catalyst for different initial CO coverages, Figure 3a. The CO coverages were measured relative to the saturated surface. At 320 K, the saturation coverage of CO on Ni(111) is a c(4 × 2)-CO structure with a coverage of 0.50 monolayer (ML),[24] where 1 ML corresponds to one CO molecule per Ni atom in the surface. All TPD experiments were performed using a heating rate of 2 K/s.

From the three lowest coverage TPDs, an Arrhenius plot was constructed. Assuming a first-order desorption $r = \nu \exp(-E_a/RT)\theta_{CO}$, plotting the reciprocal temperature versus the logarithm of the rate divided by the coverage one should obtain a straight line with a slope of $-E_a/R$ and an intercept with the y-axis of $\ln(\nu)$, see Figure 3b. Due to interactions between CO molecules on the surface, both E_a and ν will depend on coverage; for that reason we have estimated E_a and ν from very low coverage TPDs of <0.04 ML where CO interaction on the surface should be negligible, although at this low coverage we could be probing the steps on the surface, providing CO is more stable along a step which density functional theory (DFT) calculations indicate.[8] From the Arrhenius plot of the 0.011 ML CO, we can extract an activation energy barrier for CO desorption of $E_a = 119 \pm 2$ kJ/mol and a preexponential factor of $\nu = (3 \pm 1) \times 10^{13}$ s^{-1}. Only one CO peak was present in the TPDs corresponding to molecular CO desorption at relatively low site coverage. On the saturated surface, we observed a second very broad feature at around 600 K indicating a recombination of dissociated CO, see Figure 3a. To be certain we obtained the saturated structure, we cooled the sample from around 375 K in an atmosphere of CO, and it is very likely that the CO dissociation we observe happened during the first few minutes of cooling where both the CO coverage and temperature were high.

Dissociation of CO does not take place on low index surfaces below the desorption temperature of CO.[7] This is, however, not true for high index surfaces. It is believed that steps, kinks, and other surface defects lower the dissociation energy of CO.[7−8] Erley and Wagner[7] did CO TPD on both a Ni(111) surface and a stepped Ni surface. On the stepped surface, an additional CO peak appeared, believed to be a recombination of carbon and

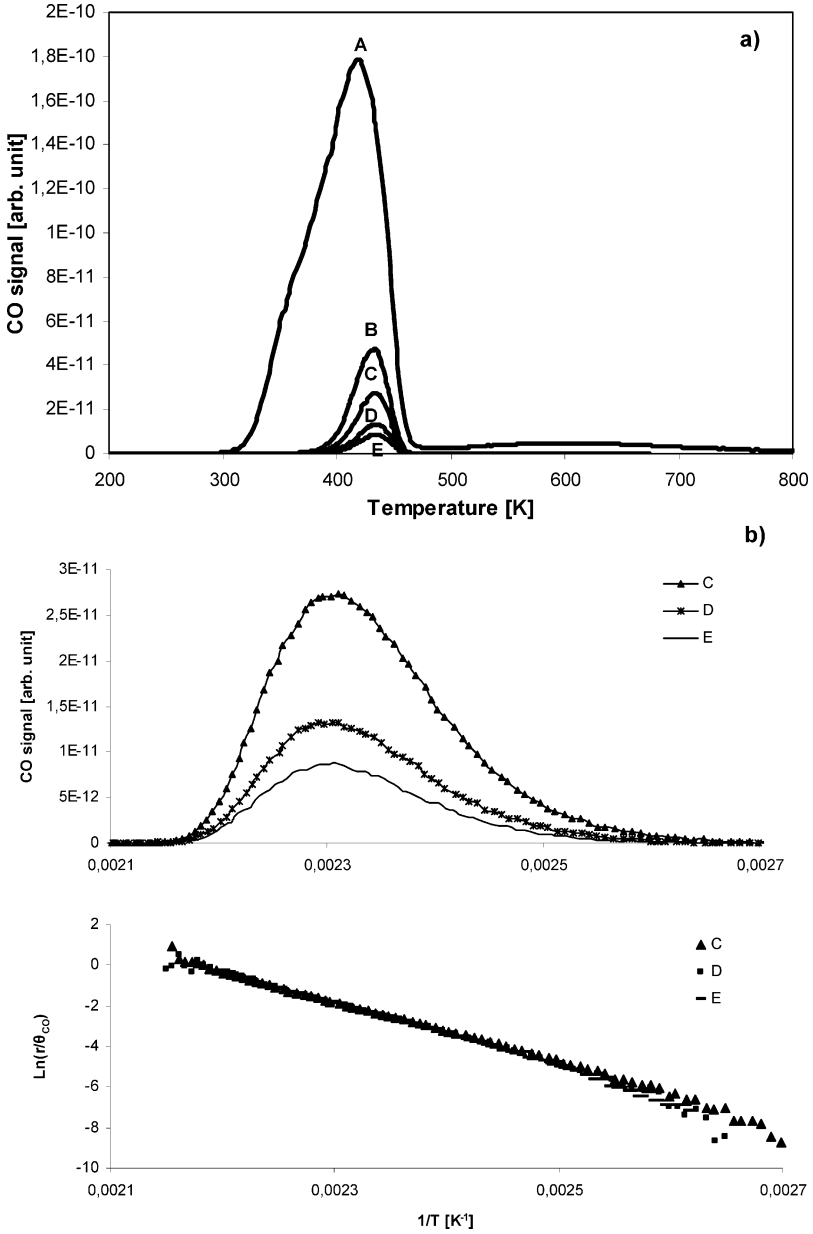

Figure 3. (a) TPD spectra for different CO coverages (given in ML) on a Ni(14 13 13) catalyst using a heating rate of 2 K/s: (A) 0.500 ML, (B) 0.064 ML, (C) 0.035 ML, (D) 0.017 ML, (E) 0.011 ML. (b) TPD spectra of low coverage CO experiments C−E plotted against 1/*T* together with an Arrhenius plot.

oxygen on the surface. According to Erley and Wagner, CO is adsorbed molecularly but dissociates at elevated temperature on the steps due to the low activation energy for dissociation on steps versus the flat surface.

Recent work by Abild-Pedersen et al.[25] indicates that CO only dissociates at the nickel steps. At the same time, carbon reconstructs the surface and grows in islands out from the steps, freeing the steps for more CO dissociation until a certain amount of carbon is produced which totally covers the steps. This island structure of the carbon is also observed by Nakano et al.[10] and Klink et al.[26] DFT calculations by Abild-Pedersen et al.[25] indicate that the CO coverage on the surface is of great importance: with a high CO coverage on the steps, interactions between the CO molecules destabilize the CO molecules and the binding energy of CO to nickel is reduced. Based on the CO coverage, the activation barrier for dissociation can vary from 100 to 220 kJ/mol.

One purpose of using a 4% stepped Ni crystal was to try to distinguish between dissociative adsorption on steps and terraces. The CO TPD experiments given in Figure 3 resulted in only one peak for CO desorption. A second peak was only observed with a high adsorption temperature (375 K) and resulted from a recombination of dissociated CO. Abild-Pedersen et al.[25] state that dissociation of CO only happens at a temperature higher than the desorption temperature of CO on Ni(111) at around 375 K[8] and that a certain pressure of CO is needed. Only one CO desorption peak indicates that the binding energy of CO to the step is not hugely different from that of CO on the terraces. There can still be a difference; it is just not big enough to distinguish a second desorption peak. The second peak is only expected to be 4% of the main peak, and it is therefore not expected to be seen if the shift is below about 50 K, corresponding to ∼20 kJ/mol.

The CO desorption peak is located around 440 K for all the low coverage experiments (Figure 3a, curves B−E). At high CO coverage, both a broadening of the desorption peak and a shift to lower temperature are shown. This behavior was also reported previously.[27−29] The peak shift and the broadening of

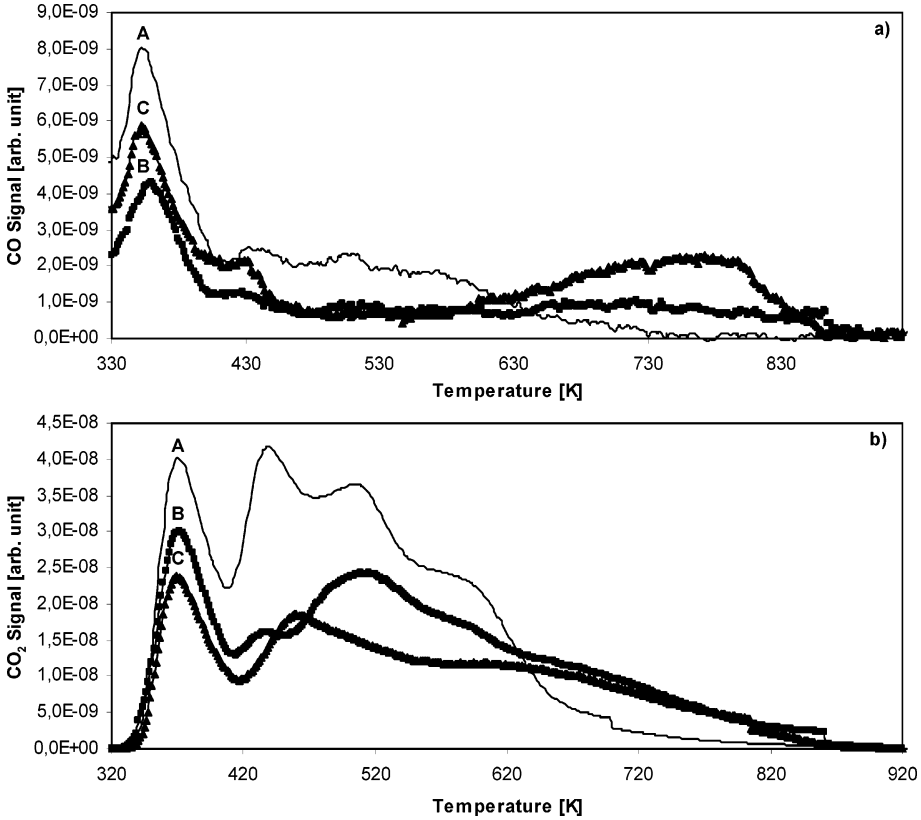

Figure 4. Desorption of CO (a) and CO_2 (b) during CO TPD experiments over the three different catalysts: (A) NiOHT30, (B) NiOHT50, (C) NiOHT70.

the peak indicate lateral interactions leading to a coverage dependence of the activation energy, E_a. The broadening of the high coverage peak can also indicate structural changes in the CO layer as observed by Held et al.[24]

Zhu et al.[30] found an activation energy for CO desorption, E_d, on Ni(111) of 106.7 kJ/mol for CO coverages of $0.1 < \theta_{CO} < 0.9$ (high coverage). Skelton et al.[31] achieved a value for E_d equal to 130 ± 5 kJ/mol. From the BOC theory, we have calculated E_d to be 122 kJ/mol using a binding energy of carbon to nickel of 715 kJ/mol. An activation energy for desorption equal to 119 kJ/mol is found experimentally for the low coverage peaks in the present work as shown in Figure 3b. Using BOC theory, we find the binding energy of C to Ni to be 703 kJ/mol on the Ni(111) surface. At high coverage, the activation energy for desorption is lowered slightly. This coverage dependence is also observed by Christmann et al.[32] for the Ni(111) surface, who saw a decrease in the activation energy of desorption from 110.8 to 98.3 kJ/mol with the CO coverage increasing from 0 to 1/3.

TPD of CO on Supported Nickel Catalyst. TPD of CO on Ni catalysts is thoroughly studied in the literature.[33−36] Hu and Ruckenstein[33] studied TPD of CO on NiO/MgO. They found that both CO and CO_2 were desorbing from the surface during the experiments. At low temperature (323−473 K), they obtained two overlapping peaks of CO and no CO_2. These peaks were believed to be molecular adsorbed CO. At higher temperature (>673 K), they got peaks for both CO and CO_2. The high temperature peaks were attributed to CO species dissociatively adsorbed on Ni. A fraction of these dissociatively adsorbed species of CO are converted to CO_2 by the following equations:

$$2CO \rightarrow 2C + 2O \rightarrow CO_2 + C \qquad (4)$$

The other fraction of CO dissociatively adsorbed desorbs as CO.[33]

Zagli et al.[35] also found that both CO and CO_2 desorbed from the surface during TPD. More than half of the adsorbed CO decomposed to yield CO_2 and surface carbon via the mechanism described in Table 2 (r_2-r_5). CO_2 desorption is the result of a reaction-limiting step, the combination of *CO and *O (r_4 in Table 2).

Galuszka et al.[36] concluded that CO disproportionation is controlled by the dissociation of CO at temperatures below 475 K, while at higher temperatures the rate is limited by the combination of *CO and *O on the surface (r_4 in Table 2). Lee et al.[34] found four CO desorption peaks during TPD over a Ni/SiO_2 catalyst. Three of them were assigned to different binding of CO to the surface, and the fourth to the recombination of carbon and oxygen. One CO_2 peak was observed at low catalyst loading, and two at high catalyst loading. The authors believed that the first peak is surface oxygen reacting with surface CO (r_4 in Table 2), and the second peak is CO readsorbing and reacting with surface oxygen via an Eley−Rideal type mechanism. However, this mechanism is not experimentally proved.

Figure 4 shows the results from CO TPD over the supported catalysts. As compared with previous data,[33−36] both CO and CO_2 desorb during TPD, but the CO_2/CO ratio (>6) is larger than reported elsewhere. One large CO peak is observed at around 350 K for all the three catalysts. For NiOHT70, a wide peak is found at 760 K. Comparing these results with previous data, the kinetics of the first peak is probably controlled by CO desorption, while the peak at high temperature is a recombination of surface carbon and oxygen, kinetically controlled by surface reaction kinetics. The high temperature peak indicates the presence of sites with a strong carbon to nickel binding energy.

The mechanism for the surface reactions and desorption from the surface is given in Table 2. The surface **CO_2 is formed in a reaction between *O and **CO. The ratio between desorbing CO_2 and CO being large indicates that a large amount

of CO is dissociated on the surface. For CO_2 desorption, four peaks are observed for NiOHT30 and NiOHT50, and three peaks for NiOHT70. All three catalysts have one large peak at around 370 K. The other peaks are in the area between 440 and 660 K. The fact that the first peak is at a very similar temperature for all three catalysts indicates that the desorption is rate controlling at low temperature. This must also mean that CO_2 is available on the surface for desorption. CO on the surface could be reacting with oxygen from dissociated CO giving CO_2 at low temperature. At temperatures above 420 K, the surface reaction kinetics seems to be rate determining.

It was found that it is very difficult to model the TPD experiments on the supported catalysts mainly due to the following reason: CO can be dissociatively or undissociatively adsorbed. The surface can consist of adsorbed **CO, **C, O*, and also adsorbed **CO_2 which is normally very low. It is therefore mathematically very difficult to define the initial conditions of the model.

TPO on Supported Nickel Catalyst. Temperature-programmed oxidation was performed in an oxygen atmosphere after CO TPD to remove residue carbon on the surface, in order to determine the amount of carbon residue and the carbon bond strength distribution of different active sites. The kinetics of carbon removal by oxygen is the topic for several literature surveys.[37−41] A primary question in these surveys is whether CO or CO_2 is the primary product during the oxidation of surface carbon.[37] In the present experiments, CO_2 is the main desorbing product (CO_2/CO > 15/1). CO_2 can also be the secondary product from CO reacting with surface oxygen.[42] Vastola et al.[43] proposed the following reaction for primary CO_2 production:

$$*CO \rightarrow *CO_2 + *C \quad (5)$$

Marsh and Foord[41] proposed the following sequence where $C(O_2)^s$ means stabilized molecular oxygen which dissociates into mobile atomic species $C(O)_m$. CO_2 is formed by interaction between these mobile species:

$$C + O_2 \rightarrow C(O_2)^s \quad \text{and}$$
$$C(O_2)^s \rightarrow C(O)_m + C(O)_m \rightarrow C + CO_2 \quad (6)$$

Finally, Du et al.[40] proposed a step where surface carbon is directly oxidized by O_2:

$$C + O_2 \rightarrow CO_2 \quad (7)$$

The fact that CO_2 emission is dominant also during TPD experiments in the absence of O_2 as shown in Figure 4 indicates that the proposal of Marsh and Foord[41] and Du et al.[40] is unlikely. The model used in this work is described in Table 2 by the equations r_1-r_5. Surface carbon combines with atomic oxygen on the surface giving surface **CO. **CO reacts further with surface *O leading to **CO_2 which desorbs:

$$**C + O* \rightarrow **CO \quad \text{and} \quad **CO + O* \rightarrow **CO \quad (8)$$

The experimental and modeling results are shown in Figure 5. The NiOHT30 and NiOHT50 catalysts have a large and sharp peak for CO_2 desorption at around 380 K. All three catalysts have wide peaks in the region around 450−500 K and a peak at high temperature (650−730 K). This last peak is large for both the NiOHT30 and NiOHT70 catalysts, indicating that much carbon is strongly adsorbed.

The modeling of the TPO experiments for all three catalysts fitted well to the experimental results. Readsorption is included in the model and does not seem to be of any great importance.

In the TPO model, the binding energy of carbon to nickel is changed, giving a spectrum of desorption peaks, which is weighted to fit the experimental data. Based on a calibration of the CO_2 signal from the mass spectrometer, good quantitative data are obtained in the experiments. The initial amount of carbon on the surface is calculated based on the total amount of CO_2 desorbing and the available surface area of Ni. Based on the modeling results, the site coverage of carbon can be plotted against the binding energy of carbon to nickel as shown in Figure 6. These results show that the amount of carbon residue on NiOHT30 and NiOHT50 is about 2 times higher than on NiOHT70.

By changing the rate constants for the different reactions in the model and doing a sensitivity analysis, we see that the recombination of **C and O* is the rate-determining step.

Since we did not model the CO TPD, it is difficult to quantitatively compare TPD and TPO results. If we qualitatively compare the two, we see several peaks for CO_2 desorption in both cases. In Table 3, we see that NiOHT30 has twice the metal surface area compared to NiOHT50 and NiOHT70. This is reflected in the TPD results (Figure 5), while in the TPO results (Figure 6) we see that the Mg^{2+}/Al^{3+} ratio seems to decrease the amount of CO_2 desorbing independent of the metal surface area on the catalysts. One possible explanation is that lowering the Mg^{2+}/Al^{3+} ratio leads to less strong carbon binding sites.

According to Hu and Ruckenstein,[33] CO_2 adsorbs on MgO sites in a NiO/MgO solid solution catalyst. In our catalyst, much of the Mg exists as Mg−Al spinel. We therefore assume that support interactions and spillover effects are small. However these effects cannot be excluded. Based on the data by Hu and Ruckenstein,[33] a spillover effect, where CO_2 is adsorbed on MgO sites, would affect the CO_2 desorption at low temperature (the low temperature peak for CO_2 desorption in Figure 4 and maybe also Figure 5).

Distribution of Active Sites on Supported Ni Catalysts. CO desorption from supported and unsupported metals has been studied by several groups as described above. Falconer and Schwarz[44] concluded that little, if any, comparison could be made between the studies of CO desorption from supported and unsupported metals. Lee et al.[34] studied desorption of CO from Ni/SiO_2 expecting support effects to be minimized and that correlation to data from unsupported catalysts might be possible. Lee et al.[34] found similarities between their data and data from single-crystal studies in the temperature range between 375 and 625 K. Outside this range, they concluded that the properties of the dispersed metal dominate the CO desorption spectra. Lee et al.[34] claim that the difficulty of making direct comparisons between results of TPD experiments with supported metals and results with unsupported metals arises mainly due to readsorption.

It has been found that CO generally adsorbs dissociatively on the transition metals listed in the upper left corner of the periodic table and molecularly on the transition metals listed in the lower right corner. Ni is close to the border separating the transition metals, so the structure of the surface is expected to affect the adsorption behavior of CO.[45] Several publications have concluded that CO dissociates at steps on unsupported nickel catalysts.[7,8,10,25] Whether CO adsorbs dissociatively at 313 K or dissociates when the catalyst is heated is not an established fact, but recent work by Abild-Pedersen et al.[25] shows that higher

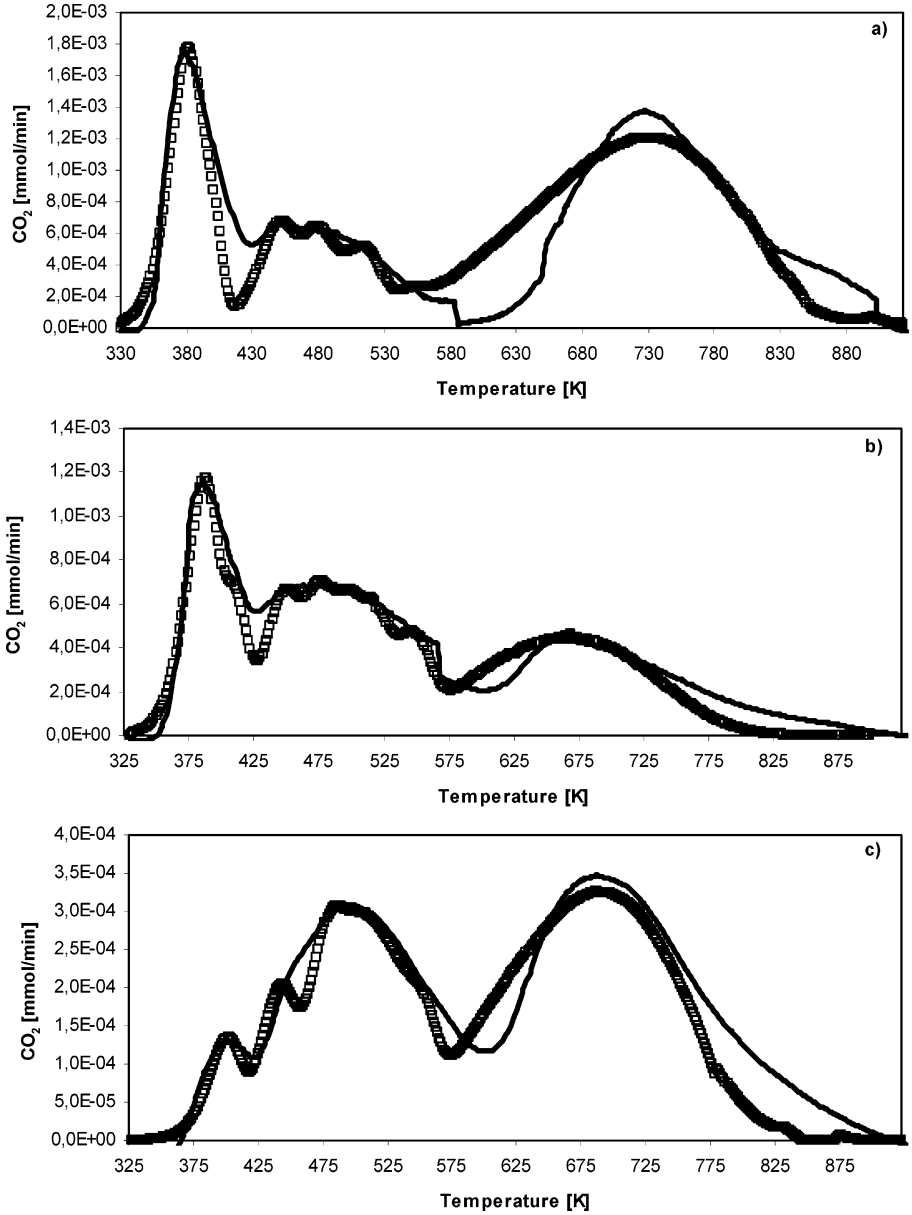

Figure 5. Experimental and model flow of CO_2 during TPO over the three different catalysts: (a) NiOHT30, (b) NiOHT50, (c) NiOHT70. Lines (−) are experimental results, and open squares (□) are model results.

temperature and a relatively high pressure of CO are needed for dissociation. The fact that CO dissociates on steps means that the activation energy for dissociation is lower on steps compared to ideal surfaces. This explains why we observe a large fraction of CO_2 during TPD of CO only on supported catalysts, where CO is adsorbed at much higher pressure compared to under UHV conditions.

Isett and Blakely[46] have used the CFSO−BEBO (crystal field surface orbital−bond energy bond order) method to calculate binding energies of C to different Ni surfaces. On the Ni(100) surface, the C is bound to 4 Ni atoms, having a binding energy of ∼715 kJ/mol. On the Ni(111) surface, the C is bound to three Ni atoms in two possible ways with binding energies of 515 and 640 kJ/mol, respectively. An experimental value for the binding energy on Ni(111) was found to be 715 kJ/mol,[47] and this is the value used in the BOC theory. On a stepped Ni (S) (7(100) × (133)) surface, the binding energy was found by Isett and Blakely[46] to be ∼757 kJ/mol. By using DFT calculations, Bengaard et al.[8] found that CO is more strongly bound to a Ni(211) surface compared to Ni(111). From this, it is concluded that carbon is more strongly bound to the stepped Ni surface compared to Ni(111).

On a real catalyst, there will be steplike sites, kinks, and defects. The fraction of different surface sites on the catalyst will determine the average binding energy of carbon to the surface. A high carbon binding energy will therefore indicate a surface with a high fraction of steplike sites, kinks, and other defects. The carbon residue after TPD is bound to the strong binding sites on the surface. The data in Figure 6 therefore only give information about the binding of carbon to the strong binding sites (in our model we consider the C to occupy 2 Ni atoms on the surface (**C), while in Figure 6 the carbon coverage is considered as 1 carbon occupying 1 Ni atom (*C)). Knowing this, it should be possible to say something about the amount of steps and maybe identify the different steplike surfaces on the catalyst.

In Figure 6, we see that the binding energy is divided into three regions. First there is a region with high binding energy in the area around 780 kJ/mol (region 1 in the figure) corresponding to the high temperature peak in Figure 5. Second

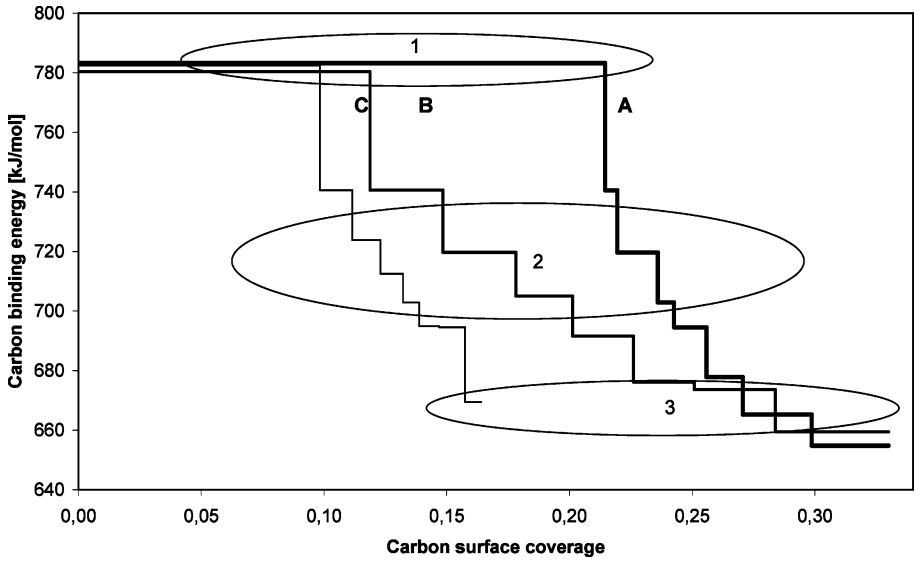

Figure 6. Carbon binding energy to the Ni surface as a function of the surface coverage of carbon for the three different catalysts: (A) NiOHT30, (B) NiOHT50, (C) NiOHT70.

there is a mediate region (region 2) with binding energies between 700 and 740 kJ/mol. In the lowest part (region 3), we have a binding energy of around 660 kJ/mol. If these results are compared to the theoretical calculations done by Isett and Blakely[46] and the results from the single-crystal TPD, it may be possible to say something about the types of surfaces present on the catalysts. The binding energy of region 2 is in the same range as the carbon binding energies on Ni(111) from both our experiments and the calculations. The mediate region seems to consist of two types of stepped surfaces. The high binding area has a binding energy in the same range as the stepped surface investigated by Isett and Blakely.[46] A relatively low binding energy was found at relatively high surface coverage, where interactions between adsorbed species and possible effects of spillover to MgO cannot be excluded. If we take this into account, we can set the whole energetic map of the supported catalysts, where sites with site coverage higher than region 2 in Figure 6 have approximately identical binding energy to the ideal surface: around 703 kJ/mol.

By comparing the data in Table 3, we see that NiOHT70 is the catalyst that gives the lowest amount of residue carbon (per m^2 Ni) after TPD. The XRD and chemisorption experiments give a trend of decreasing dispersion and increasing particle size of Ni when going from NiOHT30 to NiOHT70. A low Mg^{2+}/Al^{3+} ratio yields small particles with large dispersion, which seems to result in more steplike sites, kinks, and defects.

Conclusions

Characterization of the supported Ni catalysts by XRD, chemisorption, and TPR show that dispersion of Ni decreases with increasing Mg^{2+}/Al^{3+} ratio in the hydrotalcite-like support. The difference in dispersion could be explained by the incorporation of Ni in the hydrotalcite structure prior to calcination.

CO TPD experiments on a Ni single crystal with approximately 4% steps result in one desorption peak. It seems that dissociation of CO needs relatively high temperature and high pressure even on steps. The activation energy for desorption was 119 kJ/mol, and the binding energy of C to the Ni(111) surface was 703 kJ/mol.

Experiments with CO TPD on three different supported Ni catalysts lead to desorption of both CO and CO_2, with the latter being dominant. CO dissociation takes place, and considerable amounts of residue C are left on the surface.

TPO has been successively used to characterize the carbon layer on the surface. By using detailed kinetic modeling, a map of carbon−Ni binding energy can be obtained as a function of site coverage.

A low Mg^{2+}/Al^{3+} ratio in the hydrotalcite precursor seems to result in more steplike sites, kinks, and defects for carbon dissociation.

Directly comparing the TPD results from supported and unsupported catalysts is difficult, but the C binding energy can give an indication of the surface structure of the supported catalyst. A strong binding energy of C indicates steplike sites, kinks, and defects.

Acknowledgment. The financial support from the Norwegian Research Council through the KOSK program, Statoil, and the Danish Research Agency through the Center of Excellence "Towards a Hydrogen-based Society" Grant No. 2052-01-0054 is greatly acknowledged.

References and Notes

(1) Rostrup-Nielsen, J. R. *Catal. Today* **1994**, *18*, 305−324.
(2) Chen, D.; Lodeng, R.; Omdahl, K.; Anundskas, A.; Olsvik, O.; Holmen, A. *Stud. Surf. Sci. Catal.* **2001**, *139*, 93−100.
(3) Trimm, D. L. *Catal. Today* **1999**, *49*, 3−10.
(4) Trifiro, F.; Vaccari, A.; Clause, O. *Catal. Today* **1994**, *21*, 185−196.
(5) Tsyganok, A. I.; Tsunoda, T.; Hamakawa, S.; Suzuki, K.; Takehira, K.; Hayakawa, T. *J. Catal.* **2003**, *213*, 191−203.
(6) Cavani, F.; Trifiro, F.; Vaccari, A. *Catal. Today* **1991**, *11*, 173−301.
(7) Erley, W.; Wagner, H. *Surf. Sci.* **1978**, *74*, 333−341.
(8) Bengaard, H. S.; Norskov, J. K.; Sehested, J.; Clausen, B. S.; Nielsen, L. P.; Molenbroek, A. M.; Rostrup-Nielsen, J. R. *J. Catal.* **2002**, *209*, 365−384.
(9) Nakano, H.; Kawakami, S.; Fujitani, T.; Nakamura, J. *Surf. Sci.* **2000**, *454*−*456*, 295−299.
(10) Nakano, H.; Ogawa, J.; Nakamura, J. *Surf. Sci.* **2002**, *514*, 256−260.
(11) Chen, D.; Bjørgum, E.; Lødeng, R.; Christensen, K. O.; Holmen, A. *Stud. Surf. Sci. Catal.* **2004**, *147*, 139−144.
(12) Dumesic, J. A.; Rudd, D. F.; Aparicio, L. M.; Rekoske, J. E.; Trevino, A. A. *The Microkinetics of Heterogeneous Catalysis*; ACS Professional Reference Book; American Chemical Society: Washington, DC, 1993.
(13) Boudart, M. *Catal. Lett.* **2000**, *65*, 1−3.
(14) Shustorovich, E.; Sellers, H. *Surf. Sci. Rep.* **1998**, *31*, 1−119.
(15) Lemaitre, J. L.; Menon, P. G.; Delannay, F. *Characterization of heterogeneous catalysts*; Marcel Dekker: New York, 1984.

(16) Blekkan, E. A.; Holmen, A.; Vada, S. *Acta Chem. Scand.* **1993**, *47*, 275−280.
(17) Larsen, J. H.; Chorkendorff, I. *Surf. Sci. Rep.* **1999**, *35*, 163−222.
(18) Shustorovich, E. *Adv. Catal.* **1990**, *37*, 101−163.
(19) Holgado, M. J.; Rives, V.; San Roman, M. S. *Appl. Catal. A* **2001**, *214*, 219−228.
(20) Fornasari, G.; Gazzano, M.; Matteuzzi, D.; Trifiro, F.; Vaccari, A. *Appl. Clay Sci.* **1995**, *10*, 69−82.
(21) Shishido, T.; Sukenobu, M.; Morioka, H.; Kondo, M.; Wang, Y.; Takaki, K.; Takehira, K. *Appl. Catal., A* **2002**, *223*, 35−42.
(22) Schulze, K.; Makowski, W.; Chyzy, R.; Dziembaj, R.; Geismar, G. *Appl. Clay Sci.* **2001**, *18*, 59−69.
(23) Shishido, T.; Takehira, K. *Stud. Surf. Sci. Catal.* **2002**, *143*, 35−43.
(24) Held, G.; Schuler, J.; Sklarek, W.; Steinruck, H. P. *Surf. Sci.* **1998**, *398*, 154−171.
(25) Abild-Pedersen, F.; Remediakis, I. N.; Nørskov, J. K.; Vang, R. T.; Vestergaard, E. K.; Besenbacher, F.; Lytken, O.; Chorkendorff, I. Manuscript in preparation.
(26) Klink, C.; Stensgaard, I.; Besenbacher, F.; Laegsgaard, E. *Surf. Sci.* **1995**, *342*, 250−260.
(27) Feigerle, C. S.; Desai, S. R.; Overbury, S. H. *J. Chem. Phys.* **1990**, *93*, 787−794.
(28) Johnson, S.; Madix, R. J. *Surf. Sci.* **1981**, *108*, 77−98.
(29) Vasquez, N. J.; Muscat, A.; Madix, R. J. *Surf. Sci.* **1994**, *301*, 83−88.
(30) Zhu, X. D.; Rasing, T.; Shen, Y. R. *Chem. Phys. Lett.* **1989**, *155*, 459−462.
(31) Skelton, D. C.; Wei, D.-H.; Kevan, S. D. *Surf. Sci.* **1997**, *370*, 64−70.
(32) Christmann, K.; Schober, O.; Ertl, G. *J. Chem. Phys.* **1974**, *60*, 4719−4724.
(33) Hu, Y. H.; Ruckenstein, E. *J. Catal.* **1996**, *163*, 306−311.
(34) Lee, P. I.; Schwarz, J. A.; Heydweiller, J. C. *Chem. Eng. Sci.* **1985**, *40*, 509−519.
(35) Zagli, A. E.; Falconer, J. L.; Keenan, C. A. *J. Catal.* **1979**, *56*, 453−467.
(36) Galuszka, J.; Chang, J. R.; Amenomiya, Y. *J. Catal.* **1981**, *68*, 172−181.
(37) Li, C.; Brown, T. C. *Carbon* **2001**, *39*, 725−732.
(38) Li, C.; Le Minh, C.; Brown, T. C. *J. Catal.* **1998**, *178*, 275−283.
(39) Querini, C. A.; Fung, S. C. *Appl. Catal., A* **1994**, *117*, 53−74.
(40) Du, Z.; Sarofim, A. F.; Longwell, J. P.; Mims, C. A. *Energy Fuels* **1991**, *5*, 214−221.
(41) Marsh, H.; Foord, A. D. *Carbon* **1973**, *11*, 421−424.
(42) Hayhurst, A. N.; Parmar, M. S. *Chem. Eng. Sci.* **1997**, *53*, 427−438.
(43) Vastola, F. J.; Hart, P. J.; Walker, P. L., Jr. *Carbon* **1964**, *2*, 65−71.
(44) Falconer, J. L.; Schwarz, J. A. *Catal. Rev. Sci. Eng.* **1983**, *25*, 141−227.
(45) Broden, G.; Rhodin, T. N.; Brucker, C.; Benbow, R.; Hurych, Z. *Surf. Sci.* **1976**, *59*, 593−611.
(46) Isett, L. C.; Blakely, J. M. *Surf. Sci.* **1976**, *58*, 397−414.
(47) Isett, L. C.; Blakely, J. M. *Surf. Sci.* **1975**, *47*, 645−649.